Additive manufacturing of cermet produced by laser powder bed fusion using alternative Ni binder

Kevin Papy, András Borbély, Alexey Sova, Julien Favre, Philippe Bertrand, Jean-Marc Staerck

Materials Research Proceedings 28 (2023) 129-138 https://doi.org/10.21741/9781644902479-15

Additive manufacturing of cermet produced by laser powder bed fusion using alternative Ni binder

PAPY Kevin[1,a *], BORBELY Andras[2,b], SOVA Alexey[1,c], FAVRE Julien[2,d], BERTRAND Philippe[1,e] and STAERCK Jean-Marc[3,f]

[1]University of Lyon, Ecole Centrale de Lyon - ENISE, LTDS, CNRS UMR 5513, 58 rue Jean Parot, 42023 Saint-Etienne, France

[2]Mines Saint-Etienne, Univ Lyon, CNRS, UMR 5307 LGF, Centre SMS, F - 42023 Saint-Etienne France

[3]Technogenia, Saint-Jorioz, France

[a]kevin.papy@ec-lyon.fr, [b]borbely@emse.fr, [c]aleksey.sova@enise.fr, [d]julien.favre@emse.fr, [e]philippe.bertrand@enise.fr, [f]jean-marc.staerck@technogenia.com

Keywords: Cermet, Tungsten Carbide, Laser Powder Bed Fusion, Hot Isostatic Pressing, Microstructure, Hardness

Abstract. Cermets are composite materials made of a ceramic reinforcement and a metal matrix, generally cobalt as binder, with mass content from 6 to 20 wt.%. Cermets are produced by conventional sintering process and are known for their high hardness, low friction coefficient, high wear resistance, and high melting temperature. Laser Powder Bed Fusion (L-PBF) is an additive manufacturing technology widely applied for direct fabrication of functional metallic parts with complex geometry such as internal channels or lattices structures. Considering several studies, production of cermets by L-PBF process is challenging. Recent publications have demonstrated the feasibility to produce WC-Co parts by L-PBF combined with Hot Isostatic Pressure (HIP) heat-treatment. HIP process is sometimes additionally performed as post-treatment to remove defects. HIP is performed at high temperatures and isostatic pressures in a furnace [1]. In this study, following an experimental design a parametric optimization was conducted in order to maximize the mass density of WC-17Ni. Process parameters were compared to those used for WC-17Co parts from recent study [2]. To improve the printed specimen integrity, the as-built samples were heat-treated. As-built and HIP samples were analyzed and compared in terms of mass density, microstructure, crystallographic phases, and macro hardness.

Introduction

Laser power bed fusion (L-PBF) is an Additive Manufacturing (AM) process employed for the production of complex functional parts using metal powder as feedstock material. The powder material is spread on the build platform by the scraper and compacted by the roller. Laser beam is controlled by the scanner on the XY plane, and the platform is moved in the Z direction. Then a new powder layer is deposited, and the process is repeated until the complete part is built. The final properties of the built parts, such as roughness, porosity, cracking propensity, and mechanical properties, depend on process parameters, such as laser power P (W), scanning speed Vs (mm/s), hatching distance Hd (µm) and layer thickness l (µm) [3-8]. These factors are important because re-melting depends on the amount of the volume energy density VED (J/mm^3) absorbed during the process [9], which is defined by the following equation:

$$VED = \frac{P}{Vs \times Hd \times l} \quad (1)$$

Results in this study will only be reported in *VED* and expressed in J/mm^3. Cermets are composites material made of a hard refractory carbide embedded in a ductile metal binder matrix, usually cobalt matrix. The choice of transition metal such as Co, Fe or Ni, has been done based on their good wettability and solubility of W and C and based on their good mechanical properties. Cermets, also known as Hardmetals are extensively utilized for manufacturing of cutting tools and are classically manufactured by powder sintering [10–14]. Considering several studies, it can be concluded that L-PBF manufacturing of WC-Co parts remains challenging [15–17]. Studies show that preheating of the building plate to a high temperature is a key factor to allow the manufacturing of solid samples with reduced porosity [18]. Recently, the manufacturing of complex-shaped WC-Co parts were also demonstrated in without preheating plate [2]. Even with internal porosity and short cracks could be eliminated by post HIP treatment [19–23]. However, for developments in the field of hard metals, many studies have been conducted to find alternative materials to replace cobalt due to environmental issues related to its production. Therefore, new alternative binders are considered, especially Ni and Fe-alloys. In this study, nickel was chosen instead of cobalt. Nowadays, only a few studies based on the use of nickel as alternative binder could be found in the literature. Gu D. et al. [24–26] present different results using a mix of pure nickel and pure tungsten powder, with a particle size of 45 µm and 2.5 µm respectively. Tungsten carbide is formed by adding free carbon with a particle size of 30 µm, to obtain a tungsten carbide nickel powder with a ratio of 85wt.% W, 10wt.% Ni and 5wt.% C. First test was conducted on L- PBF process using a CO_2 laser. The following suitable parameters were chosen, a laser power of 1200W, a layer thickness of 100µm, a hatching distance of 150µm and a scan speed in the range from 800 mm/s to 1200 mm/s. Volume energy density of 83 J/mm^3 allowed to manufacture W-Ni-C by L-PBF. The samples showed a good densification level of 96,3% and the microhardness of the block-shaped WC formed at a laser scan speed of 800mm/s was 1619.7 $HV_{0.1}$, which increased to a maximum value of 1870.9 $HV_{0.1}$ by increasing the scan speed at 1000 mm/s. Different phases were observed such as the hexagonal WC and the cubic Ni_2W_4C (M_6C) phase [24,25].

Present article focuses on the AM of parts using Ni as alternative binder. First, the possibility to produce L-PBF parts was evaluated by determining the optimal process parameters. In a second step the benefits of HIP post heat treatment process will be evaluated to eliminate residual porosity and cracks. Finally, the microstructure, crystallographic phases and macro hardness will be analyzed. To compare the mechanical properties, manufacturing WC-Ni by L-PBF, was compared with sintered-HIP conventionally prepared WC-Co.

Material and Methods

Characterization of the powder.

Commercially available powder of agglomerated-sintered WC-17Ni, manufactured by spray drying by Oerlikon Metco® was used in this study. The powder was initially developed for thermal spray applications such as HVOF and HVAF. The granulometry distribution was measured using an Occhio 500XY nano particle analyzer (Occhio SA, Liège, Belgium). The particle size distribution is between 15 and 53 µm. SEM images of the particles are shown in Fig. 1. The particles have a spherical morphology. The average size of the WC grains (dark grey) is in the 1-2µm range. The carbide grains are uniformly distributed in the nickel matrix (light grey). Inductively coupled plasma mass spectrometry (ICP-MS) analysis indicates that the chemical composition of binder content was close the range stated by the supplier (C: 4.7 – 5.5, Ni: 14.5 – 19.5). In particular the measured nickel and carbon content was 20.1 wt.% and 5.1 wt.% correspondingly. X-ray diffraction was carried out on initial powder to determine the different phases. The XRD pattern shows only the WC and Ni phases in the initial powder (Fig. 1 d).

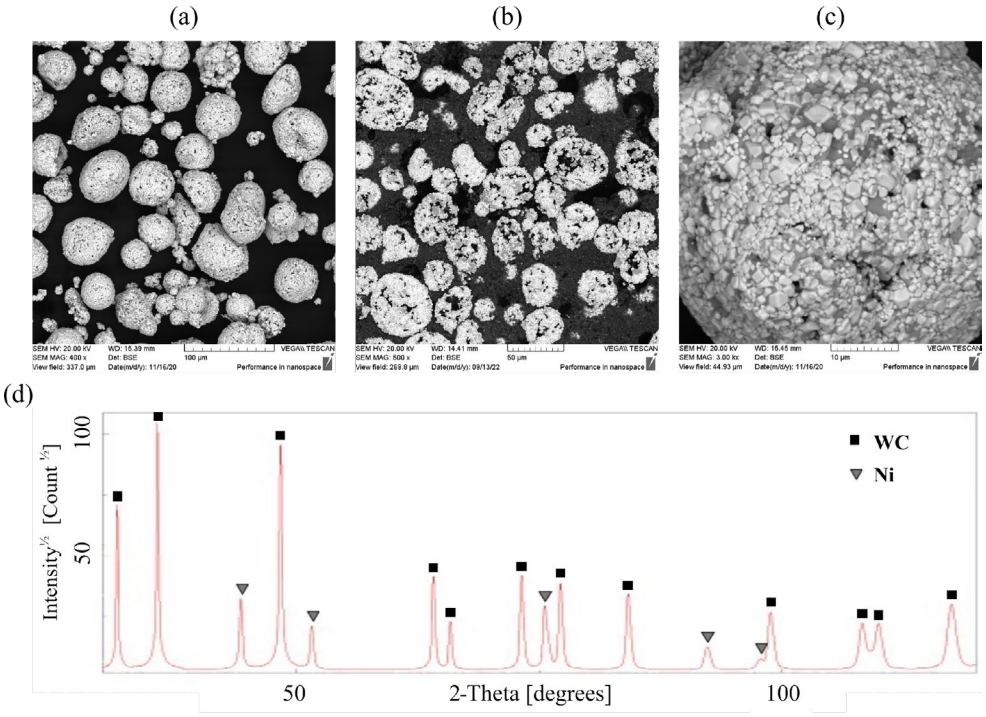

Fig. 1. SEM images of the WC-17Ni particles at different magnification (a) overview at x400, (b) cross section of particles, (c) overview at x3000 and (d) XRD pattern of WC-17Ni powder.

L-PBF and characterization equipment.

Pro X 200 DMP equipment supplied by 3D Systems® was used. The volume of the working chamber where the parts were manufactured was 140 × 140 × 125 mm^3. The L- BF machine was equipped with a 400 W fiber laser having a wavelength of 1070 nm. To prevent oxidation the working chamber was filled with nitrogen during manufacturing. Cube-shaped samples with dimensions of 10 × 10 × 10 mm^3 manufactured using L-PBF were used for post-treatment in order to reduce porosity. Samples was subjected to capsule-free HIP, which is a cycle applied during industrial processes. HIP was performed at 1450 °C with a furnace maintained at a pressure of 40 MPa for 5h. The relative density of the manufactured parts was determined by image analysis of microscope images using ImageJ [27]. The microstructure and elemental distribution were analyzed using a Zeiss Supra 55VP v2 SEM and EBSD maps were also recorded. X-ray diffraction (XRD) was employed for phase analysis using an X'PertPro MPD diffractometer with CuKα radiation. Phase quantities were obtained from Rietveld analysis performed with the MAUD software [28]. Vickers hardness (HV) was determined by applying a load of 30 kg for 10 s to all samples. Palmqvist toughness was determined by crack propagation measurement after indentation test [29].

Results and Discussion

Optimization of process parameters.

In this study, the possibility to produce cermet by L-PBF without preheated plate and the optimal process parameters will be determined. L-PBF process parameters were determined following a designed experimental optimization (DEO). Two different step was realized, first, single tracks were deposited with a powder layer thickness of 30 µm with different laser power and scan speed. Single tracks width was measured in order to determine the hatching distance.

Table 1. Ranges of L-PBF manufacturing parameters applied in the experiments.

Layer thickness [µm]	30
Laser power [W]	160 - 200 - 250
Scan speed [mm/s]	50 - 100 -150 -200 -250 -400
Hatching distance [µm]	80 - 280
Volume Energy Density [J/mm3]	160 - 650
Scan strategy	Rt - Hexagone

Then, 3D objects with simple geometries (cubes and parallelepipeds) were manufactured. The principal purpose of these experiments was to determine the parameters enabling the production of materials with the lowest amount of porosity and cracks. Table 1 summarizes the parameter ranges tested in the DEO. For manufacturing the cubes, two different scanning strategies were used, a hexagon (H) strategy, which reduces the residual stresses in the workpiece and allow creating large surfaces and a classical round trip (Rt) strategy with 90° rotation between each layer. The evolution of the porosity for WC-Ni sample is shown in Fig. 2. For a power of 160W, the porosity was the highest. Many of the cubes were not printed in full height and manufacturing was cancelled during the process. Following these observations, several parameters were set as non-optimal for this powder and parameter ranges were modified. In particular the width of VED window was decreased to 180 J/mm^3 - 300 J/mm^3 for 200W and 250W respectively. At the first stage for a VED of 200 J/mm^3 and for 300 J/mm^3, cubes with a hexagonal scanning strategy were manufactured but, the porosity was high due to inappropriate hatching distance.

For the Rt scanning strategy, samples had the lowest porosity rate of 1.06% and 0.84% for 200W and 250W respectively. Hexagonal scanning strategy shows a minimum porosity of 1.20% at 208 J/mm^3. For the lowest VED of 180 J/mm^3 porosity was the highest but it could be decreased by increasing the VED value.

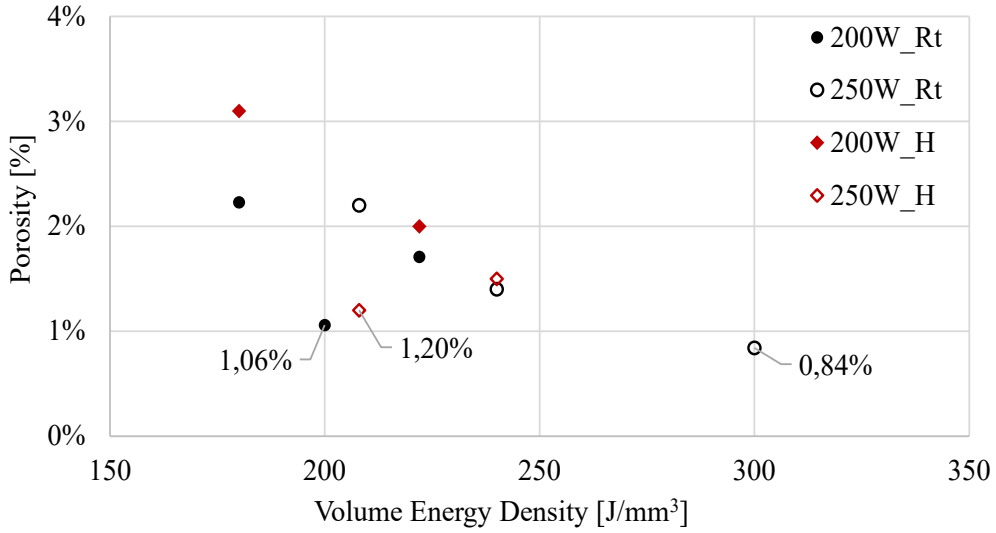

Fig. 2. Sample porosity vs. VED for round trip and hexagonal scanning strategies.

The microstructures of fabricated samples are shown in Fig. 3. Cracks are present in all samples. The smallest number of cracks is observed in the samples manufactured at VED 208 J/mm^3 and 300 J/mm^3 with a hexagonal and round-trip scan strategy respectively. During the fabrication of the samples with larger scanning surface the round-trip strategy presents some difficulties with

several defects. This problem was solved using optimized parameters at 208 J/mm^3 with hexagonal scanning strategy.

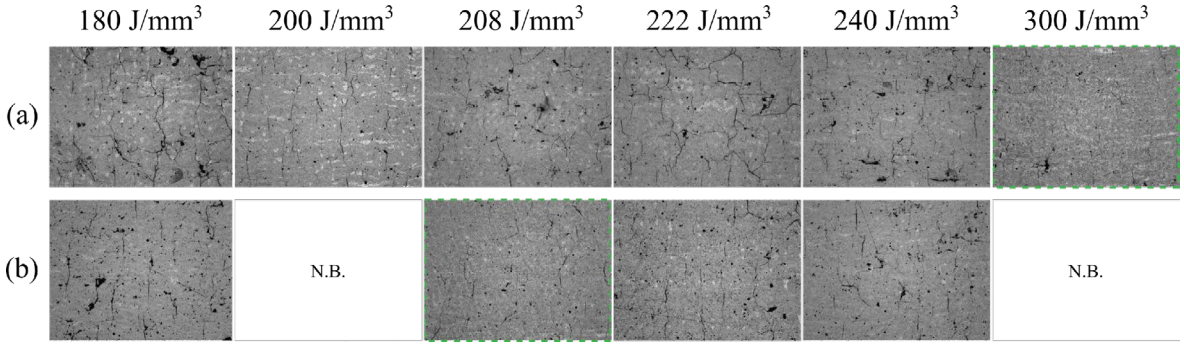

N.B. = No built

Fig. 3. SEM images of samples manufactured via (a) the round trip and (b) the hexagonal scanning strategy.

The material optimization stage determined parameters to achieve minimum porosity levels of 1.2% for WC-17Ni. In order to solve the remaining porosity problems, HIP post treatment is applied on the as-built samples (Fig. 4). HIP significantly modified integrity, microstructure and crystallographic phases. In particular, porosities and cracks were no longer visible in the images because high temperature and the external pressure promote material diffusion, allowing for pore and crack closure. According to image analysis, the relative density of the as-built samples was 98.80%, whereas of the samples after HIP post-treatment was 99.99% (Fig. 4 b).

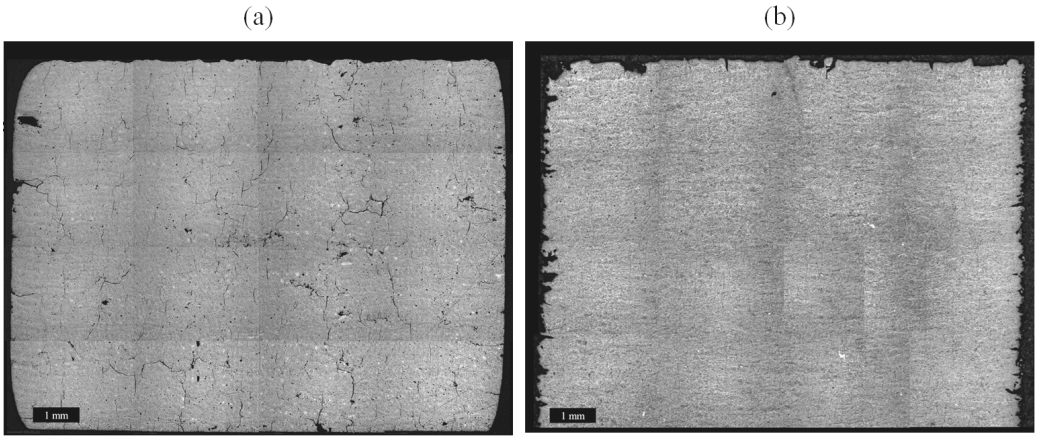

Fig. 4. Cross-section images of (a) as-built and (b) HIP-treated samples.

Microstructure and mechanical characterization.

The results of the XRD analysis performed on the as-built and HIP samples are shown in Fig. 5. The diffractograms show several phases. The most intense peaks correspond to WC.

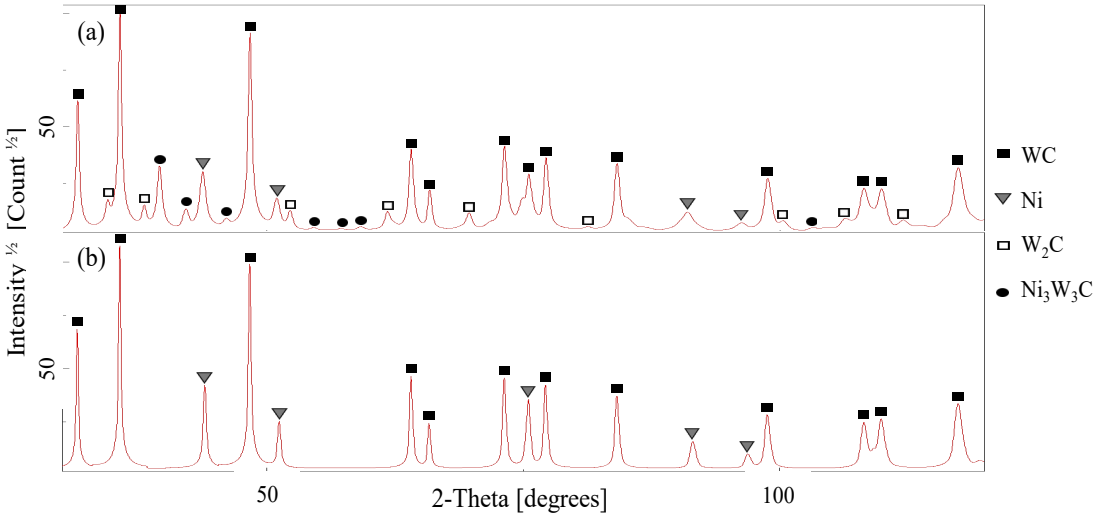

Fig. 5. XRD patterns of (a) the as-built and (b) HIP-treated samples.

At the same time the initial WC carbide has partially diffused in matrix and formed the complex phases such as W_2C carbide and the Ni_3W_3C ternary phase (M_6C). Also, the Ni matrix phase is present in the XRD pattern of the as-built sample. The XRD patterns of the HIP samples are presented on Fig. 5 b. A significant phase transformation is observed for the sample after HIP treatment. In particular, the W_2C carbide and M_6C phase have disappeared. The W-C phase diagram established by Okamoto in 2008 [30], allows to explain the disappearance of the W_2C phase. A temperature of 1450°C during HIP treatment allows the binder dissolution, then slowly cooled to room temperature, which leads to the disappearance of the W_2C phase.

EBSD analysis was performed on different samples to see the distribution of the different phases and to determine the carbide grain size. A 0.2µm step size was used and grains orientation was colored according to the inverse pole figures. No preferential orientation was observed for the samples. An indexing rate of 40% and 85% is obtained for as-built and HIP sample respectively (in Fig. 6 noise reduction was applied). The indexing rate is very low for the as-built sample (Fig. 6a), due to the presence of nano-sized grains making phase detection more difficult. A very large part of the map is non-indexed (black area), the other phases are detected but are present in very small fractions. In the as-built sample the most abundant phases are the WC phase (blue: 32.60 vol.%) and the W_2C phase (green: 9.26 vol.%). The other phases are present in area fractions lower than 1%. The phase distribution map shows a homogeneous distribution of the WC and Ni phases with a respective volume fraction of 72% and 13% for the HIPed sample. Dissolution of the smallest carbide grains is observed. The smallest equivalent WC grain size is 0.23 µm and 0.71µm for as-built and HIP sample respectively. The average grain size increases for the WC grains, from 0.60 µm to 1.58 µm for the HIP sample. The EBSD shows no preferred orientation of the WC grains in the as-built or HIP-treated material. However, a heterogeneous size distribution of WC grains is observed in both cases with zones of small and large grains (Fig. 6c and 6d). Further analysis is required to determine the preferential arrangement of the grains in the single track.

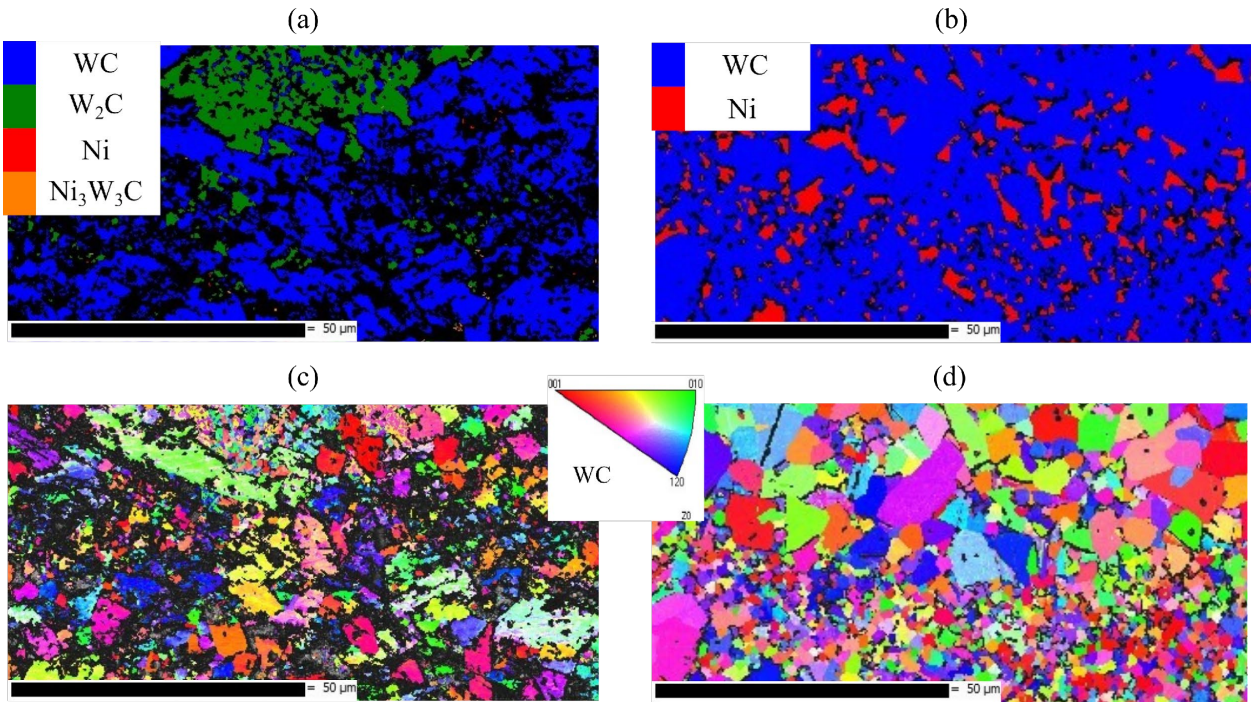

Fig. 6. EBSD grain mapping of WC-Ni (a) As-built and (b) HIP-treated sample and corresponding EBSD orientation map of WC-Ni (c) As-built and (d) HIP-treated.

Macrohardness tests were performed on the as-built and HIP-treated samples. Three measurements were performed per sample according to the standard methods at 30 kg. To reinforce the density obtained by images analysis results, the density variation of the samples is also measured by pycnometer. Results of mechanical tests are shown in Table 2.

Table 2. Characteristic values of the different WC-Ni samples.

Echantillon	Densité [g/cm^3]	HV_{30}	Tenacité Palmqvist [N.mm^{-1}]
As-built	13,94 ± 0,04	992 ± 54	1255 ± 589
HIP	14,15 ± 0,03	966 ± 21	0

Material cracking was observed near the corners of the indent for the as-built sample, which indicated high material brittleness (Fig. 7 a-b). The mean value obtained for the as-built samples was 992 HV_{30}, with a mean Palmqvist value of 1255 N.mm^{-1}. The hardness of the HIP-treated (966 HV_{30}) samples was slightly lower than that of the as-built samples. No material cracking is observed, likely due to elimination of the fragile W_2C phase (Fig. 7 c-d). Some dark points are observed on the optical image of the HIP sample, but these points do not correspond to porosities but to marks due to polishing process.

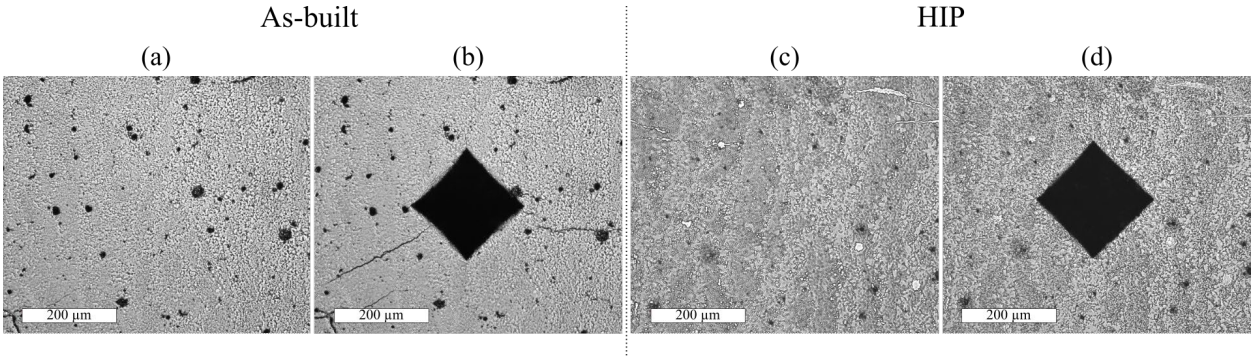

Fig. 7. Optical microscopy images of the WC-Ni samples before and after indentation tests; (a-b) as-built and (c-d) HIP-treated samples.

Summary

The manufacture of WC-17Ni parts using L-PBF was found to be feasible despite the presence of porosities and cracks. Samples with the lowest porosity fraction (1.2%) and highest integrity were obtained using a volume energy density of 208 J/mm^3. The as-built samples contained the brittle W_2C phase and some small-scale pores and cracks. The sample microstructure, relative density, and hardness were significantly improved through HIP post-treatment, resulting in close-to-zero porosity and no cracks. HIP allowed the complete dissolution of the undesirable brittle W_2C and M_6C phases. Initial phase present in the powder is observed in the sample after the HIP process. The macrohardness of the L-PBF-manufactured WC- 17Ni parts are comparable to the values obtained for the sintered WC-Co samples, with a hardness value around 1000 HV_{30}. The feasibility of L-PBF additive manufacturing to generate dense cermet samples using alternative binder as nickel was successfully assessed (Fig. 8).

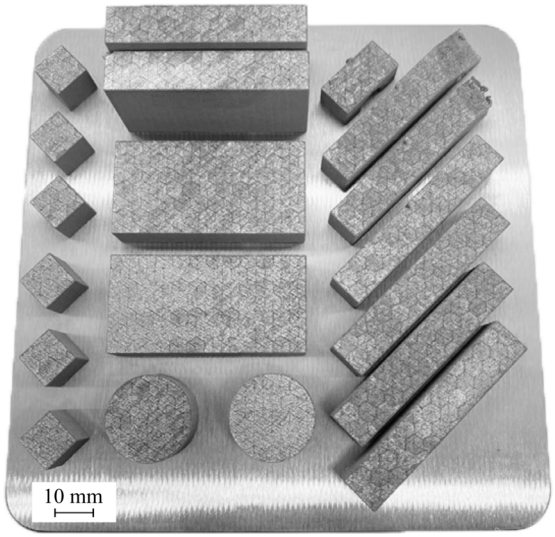

Fig. 8. L-PBF built plateform with samples manufactured from WC-17wt.% Ni powder.

References

[1] H.V. Atkinson, S. Davies, Fundamental aspects of hot isostatic pressing: An overview, Metall. Mater. Trans.: Physical Metallurgy and Materials Science 31A (2000) 2981-3000. https://doi.org/10.1007/s11661-000-0078-2

[2] K. Papy, S. Jean-Marc, S. Alexey, B. Andras, Additive Manufacturing feasibility of WC-17Co cermet parts by Laser Powder Bed Fusion, Procedia CIRP 111 (2022) 153-157. https://doi.org/10.1016/j.procir.2022.08.049

[3] E. Herderick, Additive manufacturing of metals: A review, Materials Science and Technology Conference and Exhibition 2011, MS and T'11 2 (2011) 1413–1425.
[4] N. Li, S. Huang, G. Zhang, R. Qin, W. Liu, H. Xiong, G. Shi, J. Blackburn, Progress in additive manufacturing on new materials: A review, J. Mater. Sci. Technol. 35 (2019) 242-269. https://doi.org/10.1016/j.jmst.2018.09.002
[5] B. Zhang, Y. Li, Q. Bai, Defect Formation Mechanisms in Selective Laser Melting: A Review, Chinese Journal of Mechanical Engineering (English Edition) 30 (2017) 515-527. https://doi.org/10.1007/s10033-017-0121-5
[6] S. Vock, B. Klöden, A. Kirchner, T. Weißgärber, B. Kieback, Powders for powder bed fusion: a review, Progress in Additive Manufacturing 4 (2019) 383-397. https://doi.org/10.1007/s40964-019-00078-6
[7] I. Gibson, B. Stucker, D. Rosen, Additive Manufacturing Technologies 3D Printing, Rapid Prototyping, and Direct Digital Manufacturing, Second Ed., Springer, New York, 2019. https://doi.org/10.1007/978-1-4939-2113-3
[8] C.Y. Yap, C.K. Chua, Z.L. Dong, Z.H. Liu, D.Q. Zhang, L.E. Loh, S.L. Sing, Review of selective laser melting: Materials and applications, Appl. Phys. Rev. 2 (2015) 041101. https://doi.org/10.1063/1.4935926
[9] L.N. Carter, M.M. Attallah, R.C. Reed, Laser Powder Bed Fabrication of Nickel-Base Superalloys: Influence of Parameters; Characterisation, Quantification and Mitigation of Cracking, 2012.
[10] C. Chen, Z. Guo, S. Li, Y. Xiao, B. Chai, J. Liu, Microstructure and properties of WC-17Co cermets prepared using different processing routes, Ceram. Int. 45 (2019) 9203-9210. https://doi.org/10.1016/j.ceramint.2019.01.265
[11] Z. Roulon, J.M. Missiaen, S. Lay, Carbide grain growth in cemented carbides sintered with alternative binders, Int. J. Refract. Metal. Hard Mater. 86 (2020) 105088. https://doi.org/10.1016/j.ijrmhm.2019.105088
[12] H.M. Ortner, P. Ettmayer, H. Kolaska, I. Smid, The history of the technological progress of hardmetals?, Int. J. Refract. Metals Hard Mater. 49 (2015) 3-8. https://doi.org/10.1016/j.ijrmhm.2014.04.016
[13] R.T. Faria, M.F. Rodrigues, I. de Andrade Esquef, H. Vargas, M. Filgueira, On the thermal characterization of a HPHT sintered WC-15% wt Co hardmetal alloy, Int. J. Refract. Metals Hard Mater. 23 (2005) 115-118. https://doi.org/10.1016/j.ijrmhm.2004.11.007
[14] A.S. Kurlov, A.A. Rempel', Effect of sintering temperature on the phase composition and microhardness of WC-8 wt % Co cemented carbide, Inorganic Materials 43 (2007) 602-607. https://doi.org/10.1134/S002016850706009X
[15] C.M. Fernandes, A.M.R. Senos, Cemented carbide phase diagrams: A review, Int. J. Refract. Metals Hard Mater. 29 (2011) 405–418. https://doi.org/10.1016/j.ijrmhm.2011.02.004
[16] A. Aramian, S.M.J. Razavi, Z. Sadeghian, F. Berto, A review of additive manufacturing of cermets, Addit. Manuf. 33 (2020) 101130. https://doi.org/10.1016/j.addma.2020.101130
[17] Y. Yang, C. Zhang, D. Wang, L. Nie, D. Wellmann, Y. Tian, Additive manufacturing of WC-Co hardmetals: a review, Int. J. Adv. Manuf. Technol. 108 (2020) 1653-1673. https://doi.org/10.1007/s00170-020-05389-5
[18] T. Schwanekamp, Parameter study on laser beam melting of WC- Co at 800°C pre-heating temperature, ICAT Proceedings of 7th International Conference on Additive Technologies, no. October, pp. 78-84, 2019.
[19] D. Bricín, M. Ackermann, Z. Jansa, D. Kubátová, A. Kříž, Z. Špirit, J. Šafka, Development of the structure of cemented carbides during their processing by slm and hip, Metals 10 (2020) 1-17. https://doi.org/10.3390/met10111477

[20] J. Chen, M. Huang, Z.Z. Fang, M. Koopman, W. Liu, X. Deng, Z. Zhao, S. Chen, S. Wu, J. Liu, W. Qi, Z. Wang, Microstructure analysis of high-density WC-Co composite prepared by one step selective laser melting, Int. J. Refract. Metals Hard Mater. 84 (2019) 104980. https://doi.org/10.1016/j.ijrmhm.2019.104980
[21] T. Schwanekamp, M. Reuber, Additive manufacutring of application optimized tungsten carbide precision tools, 6 th International Conference on Additive Technologies, January 2016, pp. 100–114, 2016. https://doi.org/10.1016/S0925-8388(03)00637-6
[22] T. Schwanekamp, Thermal Post-Treatment of Additively Manufactured WC-Co Processed by Laser Powder Bed Fusion, 2019.
[23] E. Uhlmann, A. Bergmann, W. Gridin, Investigation on Additive Manufacturing of Tungsten Carbide-cobalt by Selective Laser Melting, Procedia CIRP 35 (2015) 8-15. https://doi.org/10.1016/j.procir.2015.08.060
[24] D. Gu, W. Meiners, Microstructure characteristics and formation mechanisms of in situ WC cemented carbide based hardmetals prepared by Selective Laser Melting, Mater. Sci. Eng. A 527 (2010) 7585-7592. https://doi.org/10.1016/j.msea.2010.08.075
[25] D. Gu, Q. Jia, Novel crystal growth of in situ WC in selective laser-melted W - C - Ni ternary system, Journal of the American Ceramic Society 97 (2014) 684-687. https://doi.org/10.1111/jace.12828.
[26] D. Gu, In Situ WC-Cemented Carbide-Based Hardmetals by Selective Laser Melting (SLM) Additive Manufacturing (AM): Microstructure Characteristics and Formation Mechanisms, in Laser Additive Manufacturing of High-Performance Materials, Springer Berlin Heidelberg, 2015, pp. 151–173. https://doi.org/10.1007/978-3-662-46089-4_5
[27] Information on https://imagej.nih.gov/ij/ (accessed on 07 December 2022)
[28] Information on http://maud.radiographema.eu/ (accessed on 07 December 2022)
[29] “Hardmetals - Palmqvist toughness test - ISO28079.” 2009.
[30] H. Okamoto, C-W (Carbon-Tungsten), J. Phase Equilibria Diffus. 29 (2008) 543-544. https://doi.org/10.1007/s11669-008-9396-7